New Journal of Physics
The open-access journal for physics

Fluorescence enhancement through modified dye molecule absorption associated with the localized surface plasmon resonances of metallic dimers

George Zoriniants[1] **and William L Barnes**
School of Physics, University of Exeter, Stocker Road, Exeter, EX4 4QL, UK
E-mail: G.Zorinyants@exeter.ac.uk

New Journal of Physics **10** (2008) 105002 (12pp)
Received 30 April 2008
Published 28 October 2008
Online at http://www.njp.org/
doi:10.1088/1367-2630/10/10/105002

Abstract. Nano-antennae consisting of gold particle dimers were fabricated by electron-beam lithography. Dark-field scattering spectroscopy was used to probe the plasmonic response of individual nano-antennae and to characterize the localized surface plasmon resonances they support. Fluorescence from dye molecules dispersed in a thin polymer film that covered the dimers was used to probe the interaction between fluorophores and the nano-antennae. Through a suitable choice of dye emission spectrum and spectral position of the dimer resonance, we were able to focus on the way the plasmon resonances may mediate absorption of incident light by the dye. We separated out the role of plasmon resonances on absorption from emission. This was done using energy transfer in a donor–acceptor pair of dyes.

[1] Author to whom any correspondence should be addressed.

Contents

1. Introduction

Nanoparticles of noble metals are well known as efficient and wavelength-selective light scatterers [1, 2]. This resonant scattering is due to the collective oscillation of the conduction electrons in such structures, they are often known as localized surface plasmon resonances (LSPRs) [3]. Such nanoparticles open the way to a range of interesting applications including apertureless near-field probes for scattering [4], for fluorescence [5, 6] and magneto-optical microscopy [7]. Enhancement of the electromagnetic field in the vicinity of the particles also finds application in various nonlinear processes, notably surface-enhanced Raman scattering spectroscopy [8], multi-photon luminescence [9] and frequency mixing [10].

A richer range of possibilities exists when two or more metallic nanostructures are coupled, the modes associated with each individual nanostructure interact to form new hybrid modes [11, 12]. Nanoparticle dimers are the simplest of such structures and have been studied by many authors [13]–[23]. One of the motivations for such studies is the enhanced optical field that can be obtained in the gap between the two particles. The richness of possibilities that even such simple structures as dimers possess is apparent from the fact that the antisymmetric hybrid mode they can support leads to the possibility of a magnetic response and the creation of left-handed metamaterials [24, 25].

In the field of molecular plasmonics one seeks to exploit the interaction between optically active molecules and surface plasmons [26, 27], especially LSPRs [28]. One of the most extensively explored aspects is the coupling of fluorescing molecules to LSPRs. There are interesting possibilities from such a combination owing to the way in which the local density of optical states can modify the fluorescence process [29]–[35], and fluorescence in the presence of metallic dimers has received considerable attention [36]–[39]. Considering only the radiative processes involved in the fluorescence of a dye molecule in the vicinity of a LSPR supporting metallic nanostructure, fluorescence can be modified in two ways. Firstly, the incident (pump) light can couple to the mode(s) of the nanoparticle thereby mediating the absorption process—a nearby dye molecule thus can experience higher excitation intensity than it would otherwise do. Secondly, the electromagnetic field of the fluorescence that is emitted from the molecule can couple to the plasmon mode(s). Most work has concentrated on modifying the emission

process; less attention has been paid to the absorption process [37]. Here, we focus on the LSPR-mediated absorption process. We study fluorescence from dye molecules in the vicinity of a range of metallic dimers. We combine dark-field scattering spectroscopy and fluorescence measurements to monitor the effect of the LSPR on the fluorescence [40]. Separating out the roles of absorption and emission in the fluorescence process is not always easy. It can be accomplished through time-domain studies [41]; here, we show that it can also be accomplished using an energy transfer technique.

In what follows, we first describe how samples were fabricated and characterized. We then present and discuss results from a range of dark-field spectroscopy and fluorescence measurements before summarizing our findings.

2. Experimental

2.1. Fabrication of metallic nanostructures

Gold nanoparticles were manufactured by electron-beam lithography (EBL) using a dual scanning electron microscope/focused ion-beam system (FEI, Nova) equipped with an ELPHY Quantum lithography attachment (RAITH GmbH). We chose standard glass coverslips (Menzel-Gläser, no 1.5) as substrates for EBL because of their excellent optical properties, compatibility with the oil-immersion microscope objectives and because of the superior surface flatness they afford. Surface roughness was measured by an atomic force microscope (AFM) (NT-MDT, Solver PRO-M) to be less than 0.3 nm rms.

Substrates were cleaned by sonication for 10 min in acetone and propan-2-ol, dried under a stream of nitrogen and baked at 180° for 3 min to remove the adsorbed water and to improve wetting by the resist solution. The positive electronic resist, PMMA (950 kD from Microchem) was used in the form of a 2% solution in anisole (methoxybenzene). Spin-coating at 1500 rpm for 90 s resulted in a film thickness of ∼120 nm. After spin-coating, the substrates were baked for 3 min at 180 °C to remove the remaining solvent, and to anneal any small defects, it also made the polymer more robust. For EBL and scanning electron microscopy (SEM), the samples have to be conductive. To make the sample conductive, we deposited 25 nm of silver on the top of PMMA by thermal evaporation in vacuum ($<6 \times 10^{-9}$ bar), lithography being accomplished by electrons penetrating the silver layer to reach the underlying resist. After exposing the resist, the silver layer was removed using a chemical etchant (Sigma–Aldrich). Once all optical measurements were completed 5 nm of Cr were sputtered on top of the nanostructures so as to obtain the SEM images. After the resist had been exposed with the desired pattern it was developed using a 9 : 1 propan-2-ol/water mixture for 1 min, rinsed with de-ionized water for 1 min and dried in a nitrogen gas stream. After development a 50 nm thick gold layer was deposited by thermal evaporation under vacuum. To ensure good adhesion of the gold, 2–3 nm of Cr were deposited before the gold layer. Finally, lift-off was accomplished by soaking the samples in hot boiling acetone for 30 min to remove the remaining resist and unwanted metal, leaving the desired metallic nano-antennae.

Each sample consisted of similar arrays of nanoparticles. In any given array, all nanoparticles had the same nominal geometries of elliptical cylinders and the same orientation. The inter-particle gap (g) was varied, ranging from −44 nm (i.e. overlapped) to 160 nm (see figure 1). In each array, one separate row contained single isolated particles, these provide a useful reference. Dimers were separated from each other by 2.5 μm to ensure there was no

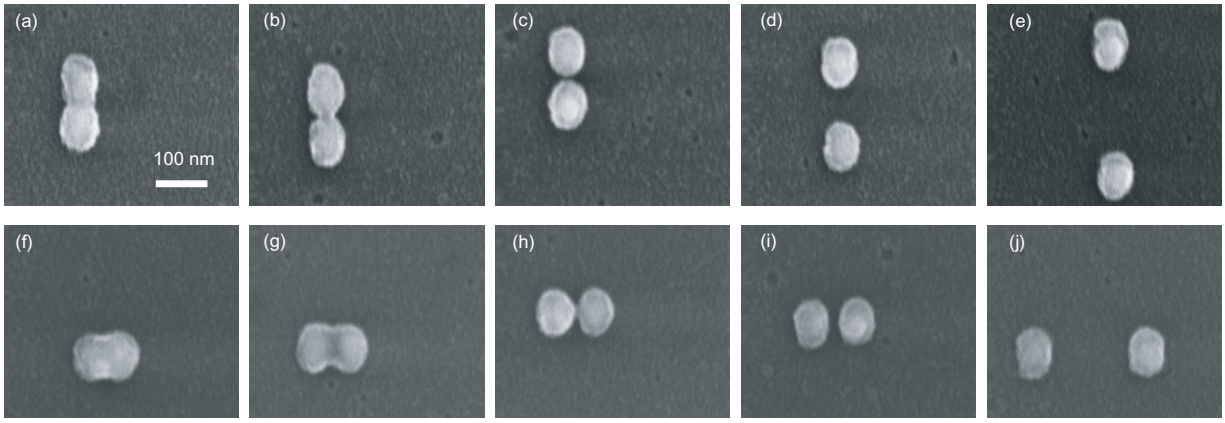

Figure 1. SEM images of gold dimer nanostructures. The particle dimensions are typically 70 nm by 95 nm; the gap size ranges from −44 to 160 nm.

inter-dimer interaction. Dimers were formed from elliptical particles in two different ways. Firstly, so that the inter-particle axis is parallel to the long axis of the ellipses (longitudinal configuration), see figures 1(a)–(e), and along the short axis (latitudinal configuration), see figures 1(f)–(i). For the optical measurements (see below) we used linearly polarized light, and thus had two orientations, parallel to the short axis of the ellipses, and parallel to the long axis; we thus had four experimental configurations.

Although produced by identical procedures, the particles showed a distribution of geometries. High-resolution SEM images (not shown) indicate that the particles consisted of nanocrystals of gold 2–10 nm in size. The exact nanocrystal structure of a given particle influences the shape of the nano-antennae, the effect becoming more important as the particle size is reduced. Structures below 100 nm in size are affected by some random shaping that is most probably due to the irregular growth of gold nanocrystals in the course of the thermal deposition. Using the techniques outlined above the minimum radius of curvature we could produce was ~ 20 nm. To characterize each nano-antenna, we used SEM data to measure the axes of each elliptical particle and to measure the gap between the particles in a given dimer. The accuracy of these measurements was limited by the resolution of our SEM to ± 5 nm.

2.2. Fluorescent dye layer

The fluorescent dyes (Oxazine 1 perchlorate and Coumarin 6) were purchased from Sigma–Aldrich and used as obtained. Coumarin 6 has an absorption band from 400 to 500 nm, peaking at 460 nm and has an emission band from 450–700 nm, peaking at 502 nm (in ethanol). Oxazine 1 has an absorption band from 580–680 nm, peaking at 642.5 nm and has an emission band that spans from 600–800 nm, peaking at 648 nm (in methanol): spectra are shown in figure 2 and based on literature data [42]. Thus, the Förster-type resonance energy transfer is possible between the two fluorophores due to the significant spectral overlap of the emission of Coumarin 6 and the absorption of Oxazine 1. At the same time, the two dyes can be separately excited by two different laser wavelengths, 458 nm (Ar-ion laser) for Coumarin 6 and 633 nm (He–Ne laser) for Oxazine 1.

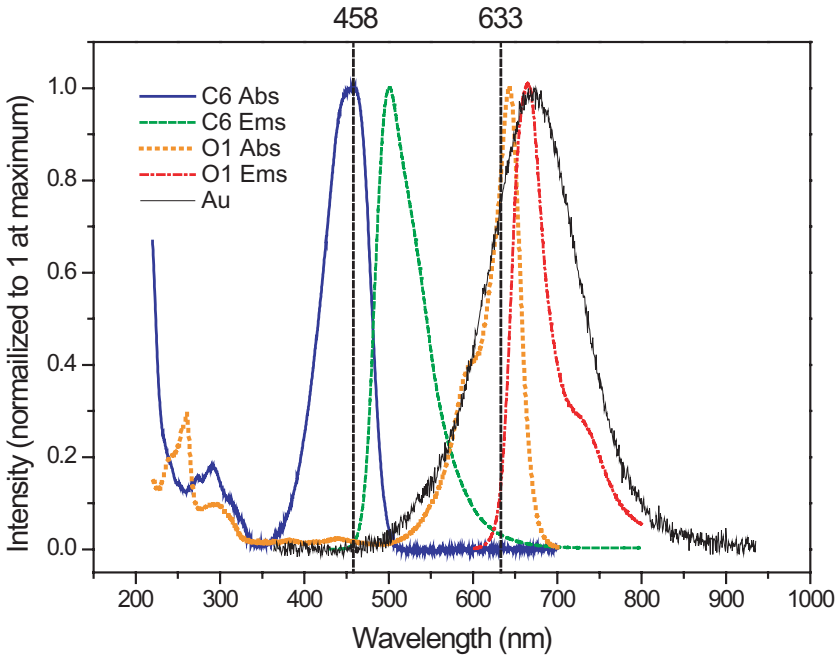

Figure 2. Absorption and fluorescence spectra of Coumarin 6 (C6) in ethanol and Oxazine 1 (O1) in methanol. Vertical lines denote the wavelengths of the lasers used. Also shown for comparison is an example of a dark-field scattering spectrum for a typical gold nanoparticle.

Both dyes were dissolved in anisole and mixed with the commercial PMMA solution. Solutions were then spin-coated on top of the nano-antennae samples. The PMMA concentration in anisole was 1% (by weight), the spinning rate 4000 rpm, and the spinning time 90 s. After drying under a nitrogen gas stream, the resulting film was ∼30 nm thick. We made films containing just Oxazine 1 (2% by weight compared to PMMA), and (for energy-transfer experiments), films containing equal amounts (1% by weight) of Oxazine 1 and Coumarin 6. The AFM measurements indicated that the dye-doped PMMA deposited as a continuous layer on the nano-antennae arrays and the emission spectra showed no evidence of dye aggregation.

2.3. Dark-field scattering and scanning fluorescence confocal microscopy

The LSPRs supported by the dimers were characterized by measuring dark-field scattering spectra. Data were acquired using a system based on a Nikon Eclipse TE2000-U inverted optical microscope and spectrometer/CCD combination (Princeton Instruments), figure 3. The particles were illuminated with a white light source (tungsten filament lamp) through a dark-field condenser. In this way, light is incident over a large angle range on the sample surface. The scattered light was collected by a 100× oil-immersion lens (Nikon) with the variable aperture (N.A. 0.5–1.25). The lens diaphragm was adjusted so as to completely block the stray light from the condenser, thus passing only the scattered light (at small angles). To ensure that the nano-antennae were measured in a homogeneous environment (thus facilitating interpretation) samples were immersed in special index-matching oil (Basildon Chemicals) to avoid dissolving the dye-doped PMMA layer.

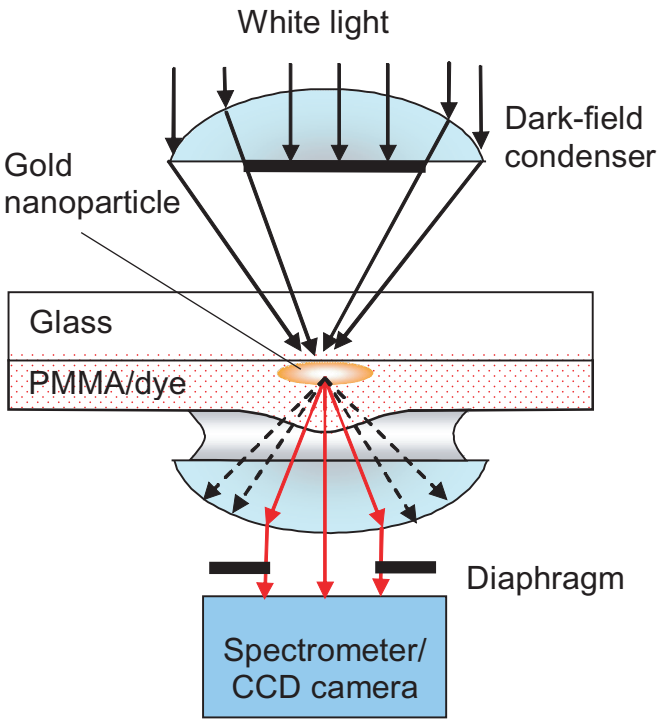

Figure 3. Schematic of the dark-field spectroscopy setup and sample arrangement for microscopy.

The images of the each individual nano-antenna were projected onto a CCD camera either using a mirror for imaging or a diffraction grating for spectroscopy. The two-dimensional CCD camera used allowed us to measure the spectra of 10–15 nano-antennae in a single run. The smallest area of sample that could be studied was about $0.5 \times 1.0\,\mu m^2$.

Fluorescence data were acquired using a Leica TCS SP5 scanning confocal fluorescence microscope. Samples were index matched to the objective oil immersion lens (Leica x63, N.A. 1.4), again so that the nanostructures were in a uniform environment. Fluorescence excitation was carried out by an integrated He–Ne or Ar-ion laser using the same lens.

3. Results and discussion

3.1. Scattering spectra of the nanoparticle pairs

Representative dark-field scattering spectra from gold nanoparticle dimers for the four dimer/polarization configurations mentioned above are shown in figure 4—the four arrangements are shown schematically in the insets. These spectra show features consistent with similar results already published in the literature, here we simply point out the significant features in the present context. For light polarized parallel to the long axis of the particles, single particles exhibit a LSPR centred at ∼730 nm, which shifts to 700 nm once the particles are connected. For light polarized parallel to the short axis of the particles there is a band centred around 550 nm. This much is as expected, however, for this polarization the long-axis resonance is also seen at ∼700 nm. We suspect that this may be due to polarization conversion of the

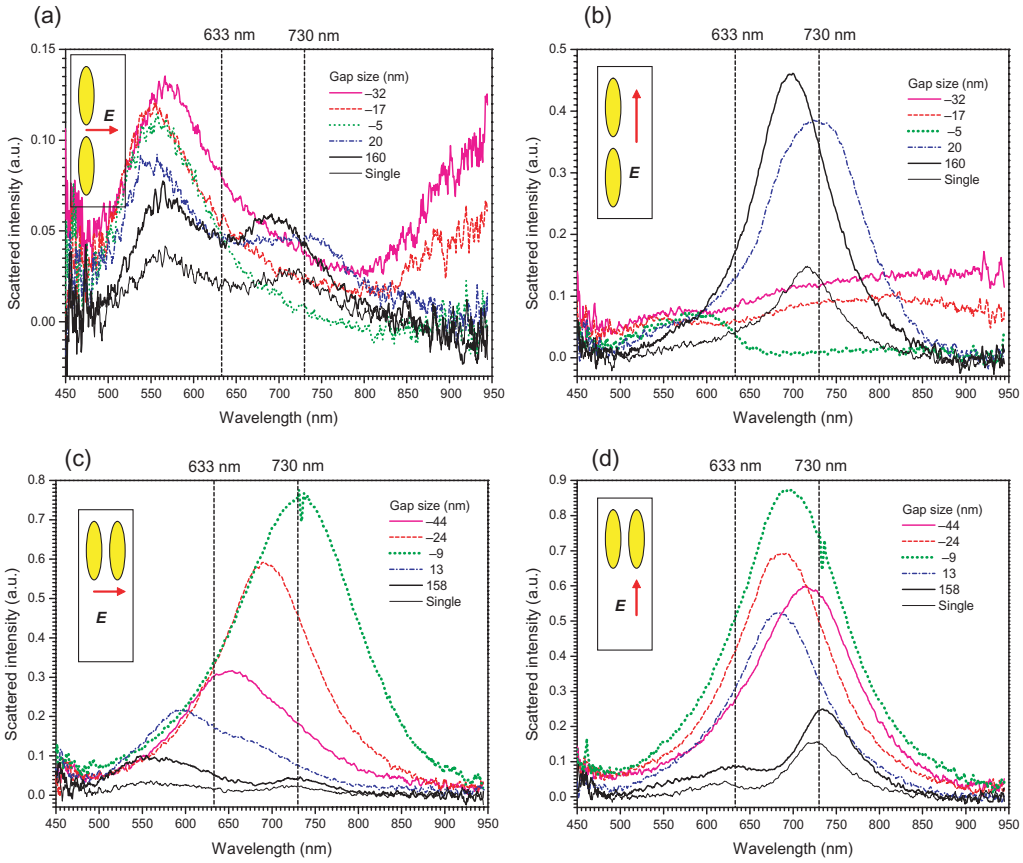

Figure 4. Dark-field scattering spectra for gold dimers for a range of interparticle separations. Four different configurations are shown that correspond to two directions of the interparticle axis and the polarization of light with respect to the long and short axes of the particles. These configurations are referred to as: (a) longitudial dimer, perpendicular polarization, (b) longitudial dimer, parallel polarization, (c) latitudial dimer, perpendicular polarization and (d) latitudial dimer, parallel polarization as indicated.

incident light by the nano-crystalline structure of the particle. (The increasing signal for some spectra in figure 4(a) at long wavelengths is an experimental artefact.)

For touching and overlapping particles, a strong change of scattering is observed only in figures 4(b) and (c). This is expected since, when a conductive bridge appears, it is parallel to the polarization of light for these configurations. In the other two cases (figures 4(a) and (d)), when the bridge is perpendicular to the electric field of the incident light, the presence of a conductive bridge does not change the length of the structure in the direction parallel to the electric field, and so there is little effect on the LSPR.

3.2. Evaluation of fluorescence enhancement

We also acquired fluorescence images of the dye-doped polymer-coated dimer structures (see figure 5(a)). From these data, we were able to extract the fluorescence enhancement due to the presence of the nanoparticle dimer. We did this by comparing the fluorescence intensity

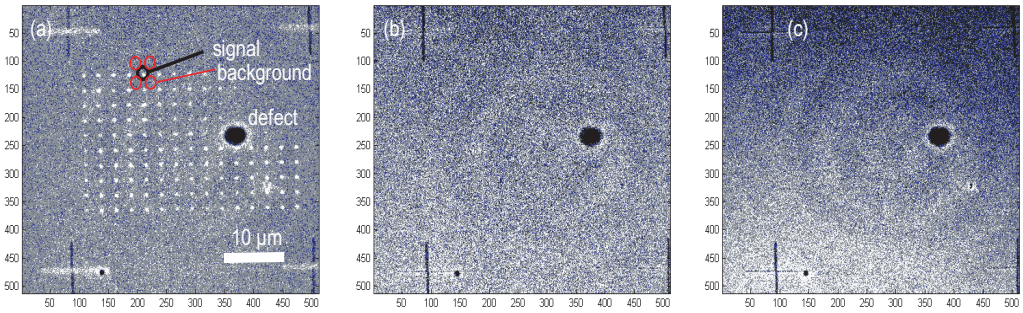

Figure 5. Comparison of confocal fluorescence images for different excitation mechanisms: (a) direct excitation at 633 nm and emission of the acceptor dye in the range 650–800 nm; (b) excitation at 458 nm and direct emission from the donor dye in the range 500–600 nm and (c) excitation at 458 nm and emission of the acceptor dye in the range 650–800 nm, i.e. the energy transfer image.

(in the emission band 650–800 nm) from the dimer region with four immediately neighbouring regions (again, see figure 5(a)). We next need to extract from data such as figure 5(a), a measure of the fluorescence enhancement (we include the possibility of reduction as well as enhancement) arising from the presence of the dimer.

The fluorescence emitted per volume of dye-doped film is proportional to the dye concentration and the local intensity of the electromagnetic field,

$$\varphi(\mathbf{r})\mathrm{d}\mathbf{r} \propto \eta \cdot \psi(\mathbf{r}) \cdot I(\mathbf{r})\mathrm{d}\mathbf{r}. \tag{1}$$

Here, $\varphi(\mathbf{r})\mathrm{d}\mathbf{r}$ is the elementary fluorescence intensity from the volume $\mathrm{d}\mathbf{r}$, η is the quantum efficiency (or quantum yield) of fluorescence, $\psi(\mathbf{r})$ is the concentration of the dye and $I(\mathbf{r})$ is the local intensity of the electric field (pump). We assume that the film of dye is thin and restrict $\mathbf{r}$ to two-dimensional space. The formula (1) is valid when the dye is far from saturation, i.e. when the fluorescence intensity is linear in excitation power. The measured fluorescence signal $F(\mathbf{r})$ is a convolution of the local fluorescence intensity $\varphi(\mathbf{r})$ given by (1) with the microscope point spread function $M(r)$,

$$F(\mathbf{r}) = [\varphi \otimes M](\mathbf{r}) = \int \varphi(\mathbf{r}')M(\mathbf{r}' - \mathbf{r})\mathrm{d}\mathbf{r}'.$$

For simplicity, let us assume that the point spread function is normalized to unity, that is,

$$\int M(\mathbf{r})\mathrm{d}\mathbf{r} = 1.$$

The measured signal S, that is the fluorescence intensity averaged in the circle of radius R, is then given by,

$$S = \frac{1}{\pi R^2} \int\limits_{r \leqslant R} F(\mathbf{r})\mathrm{d}\mathbf{r} \propto \frac{1}{\pi R^2}\eta \cdot \psi \cdot \int\limits_{r \leqslant R} \int I(\mathbf{r}')M(\mathbf{r}' - \mathbf{r})\mathrm{d}\mathbf{r}'\mathrm{d}\mathbf{r}. \tag{2}$$

For the background, the excitation intensity is uniform, $I(\mathbf{r}') \equiv I_0$, therefore (2) becomes,

$$S_{\mathrm{bg}} \propto \frac{1}{\pi R^2}\eta \cdot \psi \cdot I_0 \int\limits_{r \leqslant R} \int M(\mathbf{r}' - \mathbf{r})\mathrm{d}\mathbf{r}'\mathrm{d}\mathbf{r} = \eta \cdot \psi \cdot I_0. \tag{3}$$

The background signal is proportional to the applied field intensity and does not depend on the size of averaging circle or microscope resolution. If the collection area contains the nanoparticle then there are two contributions to the measured signal: (i) from the dye that is far from the nanoparticles and therefore is in the same uniform background and (ii) from the dye which is in the enhanced field of the nanoparticle. The size of the near-field zone is of the same order as the size of the particles (about 50 nm) [43]. This means that the fraction of the collection area covered by the near field is negligible compared with the entire collection area, therefore the background contribution from a circle containing a particle is very close to (3). Further, the resolution of the microscope is of the order of 200 nm, which means that most of the integrated intensity coming from the particle falls entirely in the circle of radius 1 μm, so in the integral (2) the finite integration area $r \leqslant R$ can be substituted by integration over the entire space. Thus, the fluorescence from the neighbourhood of the nanoparticle is given by

$$S_{\mathrm{np}} \propto \eta \cdot \psi \cdot \left(I_0 + \frac{1}{\pi R^2} \int\int I_{\mathrm{np}}(\mathbf{r}')M(\mathbf{r}' - \mathbf{r})\mathrm{d}\mathbf{r}'\mathrm{d}\mathbf{r} \right) = \eta \cdot \psi \cdot \left(I_0 + \frac{1}{\pi R^2} \int I_{\mathrm{np}}(\mathbf{r}')\mathrm{d}\mathbf{r}' \right). \tag{4}$$

Here, I_{np} is the local intensity of the total electric field near the nanoparticle. The normalized fluorescence enhancement that is the main outcome of this experiment is given by,

$$s = \frac{S_{\mathrm{np}} - S_{\mathrm{bg}}}{S_{\mathrm{bg}}} \propto \frac{1}{\pi R^2} \int \frac{I_{\mathrm{np}}(\mathbf{r}')}{I_0}\mathrm{d}\mathbf{r}'. \tag{5}$$

This means that the signal we measure is proportional to the enhancement factor of the intensity of light integrated over the volume that contains the dye. The result depends on both the field enhancement and on the size of the near-field zone; unfortunately, these two factors cannot be measured independently by this technique. Our measured enhancement factor S is thus not absolute, we refer to it as the far-field fluorescence enhancement, and it does, however, allow us to make our desired study.

3.3. Correlation between scattering efficiency and fluorescence enhancement

In figure 6, we compare the far-field fluorescence enhancement (as described above) with the scattering intensity of the different structures as a function of gap size. To analyse numerically the far-field fluorescence enhancement from images such as figure 5(a), we used the following procedure. Every bright spot in the image was surrounded by a circle with the typical diameter 1 μm. The fluorescence intensity was averaged inside the circle. Then the background fluorescence coming from the uniform parts of the dye were measured in the same way, in four circles surrounding the particular nanoparticle and interpolated it to the centre of the square. This eliminated the noise and the slow variation of the incident light intensity across the image.

If figure 6, we plot the scattering intensity at two wavelengths, 633 nm (the pump wavelength) and 730 nm (in the middle of the LSPR response—and also within the emission band of the Oxazine 1 dye). The most dramatic changes are for the longitudinal dimer, parallel polarization and the latitudinal dimer, perpendicular polarization configurations, figures 6(b)

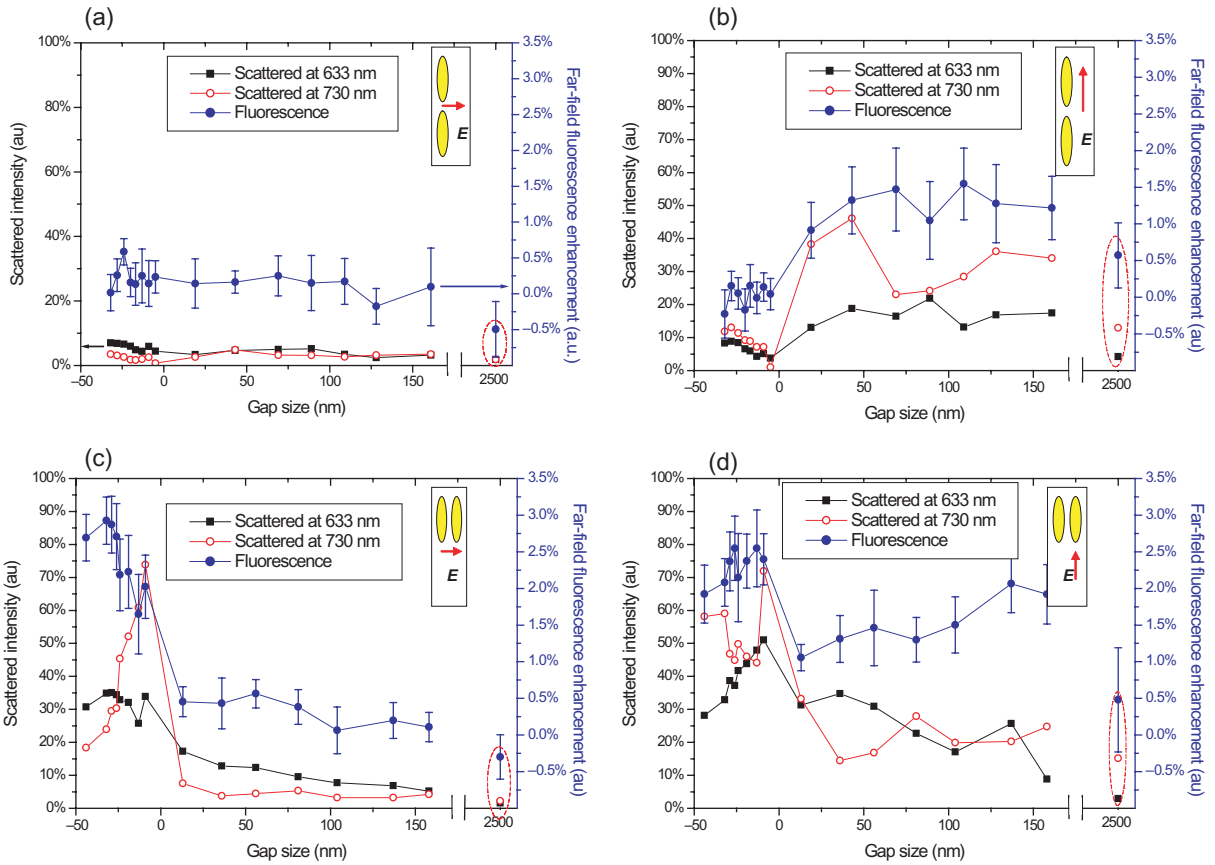

Figure 6. Scattering intensity as a function of gap size measured in the spectral bands centred at 633 and 730 nm; band width 9 nm for the four different configurations. The lines simply join the experimental data points and are included as guides to the eye. Single particles are highlighted by dashed red ellipses.

and (c). From this, the link between scattering intensity and fluorescence enhancement becomes clearer. Both scattering and fluorescence depend on the dipolar (and higher order multipolar) moment of the LSPR. The scattered intensity is proportional to the square of the dipolar moment, and the fluorescence enhancement we measure is proportional to the integrated intensity of the electric field in the volume occupied by the dye. For extremely small gap sizes, this volume may become very small. So, the measured far-field fluorescence enhancement is a result of two competing tendencies: the local fields are enhanced as the particles are closer together, and the volume of space where these fields occur shrinks. Therefore, the measured far-field fluorescence enhancement should correlate with the dipolar moment and be relatively smaller for small gap sizes.

So, comparing fluorescence and scattering data leads us to suggest that it is the effect of the LSPR on the absorption process rather than the emission process that is more important here. To test this suggestion we also investigated the emission from the same structures coated with the donor–acceptor dye combination, Coumarin 6 and Oxazine 1. We pumped the Coumarin at 458 nm, outside the absorption band of the Oxazine 1. We saw no fluorescence enhancement

when we monitored the fluorescence from the Coumarin (figure 5(b)), or when we changed our spectral window so as to collect fluorescence from the Oxazine 1 (figure 5(c)). Note that in all three images shown in figure 5 one can see the alignment marks (crosses) and a defect of the dye coating (large dust particle or air bubble). The contrast in all three images is similar, showing that there was significant fluorescence intensity coming from the acceptor dye when excited directly (a), from the acceptor dye when excited via energy transfer (c), there was also fluorescence coming from the donor dye which was not entirely quenched by energy transfer. Still, the fluorescence enhancement by the nanoparticles is seen only in the image (a). This means that we do not see enhancement that is solely due to modification of the fluorescence quantum yield. We did not observe any fluorescence quenching by direct energy transfer to metal either. Thus, we may conclude that the fluorescence enhancement results from the increase of the local excitation light intensity $I(\mathbf{r})$.

4. Conclusions

We have correlated the fluorescence enhancement with the scattering intensity for a set of individual gold nanoparticle dimers as a function of dimer gap size. We find that the fluorescence enhancement is correlated with the scattering intensity at the absorption (pump) wavelength of the dye molecules. We confirmed that, for the choice of particles and dyes used, absorption was the process being modified by the LPSRs through use of an energy transfer technique involving two types of dye molecules, donors and acceptors. This technique may find application in unravelling the roles of absorption and emission in more complex plasmon-supporting nanostructures.

Acknowledgments

We acknowledge the support through funding from the EPSRC (EP/C534689/1) and the EC (FP6-2002-IST-1–507879) for this work. WLB gratefully acknowledges the support of the Royal Society through a Wolfson Merit Award. Useful discussions with Andrew Murray and Baptiste Auguié are gratefully acknowledged.

References

[1] Kreibig U and Vollmer M 1995 *Optical Properties of Metal Clusters* (Berlin: Springer)
[2] Murray A W and Barnes W L 2007 *Adv. Mater.* **19** 3771
[3] Jensen T R *et al* 2000 *J. Phys. Chem.* B **104** 10549
[4] Zenhausern F, Martin Y and Wickramasinghe H K 1995 *Science* **269** 1083
[5] Anger P, Bharadwaj P and Novotny L 2006 *Phys. Rev. Lett.* **96** 113002
[6] Kuhn S *et al* 2006 *Phys. Rev. Lett.* **97** 017402
[7] Silva T J, Schultz S and Weller D 1994 *Appl. Phys. Lett.* **65** 658
[8] Johansson P, Xu H and Kall M 2005 *Phys. Rev.* B **72** 035427
[9] Schuck P J *et al* 2005 *Phys. Rev. Lett.* **94** 017402
[10] Danckwerts M and Novotny L 2007 *Phys. Rev. Lett.* **98** 026104
[11] Prodan E *et al* 2003 *Science* **302** 419
[12] Hohenester U and Krenn J 2005 *Phys. Rev.* B **72** 195429
[13] Rechberger W *et al* 2003 *Opt. Commun.* **220** 137

[14] Atay T, Song J-H and Nurmikko A V 2004 *Nano Lett.* **4** 1627
[15] Dahmen C, Schmidt B and von Plessen G 2007 *Nano Lett.* **7** 318
[16] Jain P K, Huang W and El-Sayed M A 2007 *Nano Lett.* **7** 2080
[17] Olk P *et al* 2008 *Nano Lett.* **8** 1174
[18] Tamaru H *et al* 2002 *Appl. Phys. Lett.* **80** 1826
[19] Muskens O L *et al* 2007 *Opt. Express* **15** 17736
[20] Muhlschlegel P *et al* 2005 *Science* **308** 1607
[21] Gunnarsson L *et al* 2005 *J. Phys. Chem.* B **109** 1079
[22] Rockstuhl C, Salt M G and Herzig H P 2004 *J. Opt. Soc. Am.* A **21** 1761
[23] Kim S *et al* 2008 *Nature* **453** 757
[24] Grigorenko A N *et al* 2005 *Nature* **438** 335
[25] Shalaev V M *et al* 2005 *Opt. Lett.* **30** 3356
[26] Dintinger J *et al* 2005 *Phys. Rev.* B **71** 035424
[27] Christ A *et al* 2003 *Phys. Rev. Lett.* **91** 183901
[28] Haes A J *et al* 2006 *J. Am. Chem. Soc.* **128** 10905
[29] Kuhn H 1970 *J. Chem. Phys.* **53** 101
[30] Drexhage K H 1974 *Interaction of Light with Monomolecular Dye Layers* ed E Wolf (Amsterdam: North-Holland) p 163
[31] Barnes W L 1998 *J. Mod. Opt.* **45** 661
[32] Girard C, Martin O J F and Dereux A 1995 *Phys. Rev. Lett.* **75** 3098
[33] Lakowicz J R 2005 *Anal. Biochem.* **337** 171
[34] Ditlbacher H *et al* 2001 *Appl. Phys.* B **73** 373
[35] Gerber S *et al* 2007 *Phys. Rev.* B **75** 073404
[36] Rogobete L *et al* 2007 *Opt. Lett.* **32** 1623
[37] Nakamura T and Hayashi S 2005 *Japan. J. Appl. Phys.* **44** 6833
[38] Zhang J *et al* 2007 *Nano Lett.* **7** 2101
[39] Bakker R M *et al* 2008 *Appl. Phys. Lett.* **92** 043101
[40] Chen Y, Munechika K and Ginger D S 2007 *Nano Lett.* **7** 690
[41] Wenger J *et al* 2008 *Opt. Express* **16** 3008
[42] Du H *et al* 1998 *Photochem. Photobiol.* **68** 141
[43] Murray A W, Suckling J R and Barnes W L 2006 *Nano Lett.* **6** 1772